

Multi-Spacecraft Analysis of Dipolarization Fronts and Associated Whistler-Wave Emissions using MMS Data

H. Breuillard,¹ O. Le Contel,¹ A. Retino,¹ A. Chasapis,² T. Chust,¹ L. Mirioni,¹ D.B. Graham,³ F.D. Wilder,⁴ I. Cohen,⁵ A. Vaivads,³ Yu.V. Khotyaintsev,³ P.-A. Lindqvist,⁶ G.T. Marklund,⁶ J.L. Burch,⁷ R.B. Torbert,⁸ R.E. Ergun,⁴ K.A. Goodrich,⁴ J. Macri,⁸ J. Needell,⁸ M. Chutter,⁸ D. Rau,⁸ I. Dors,⁸ C.T. Russell,⁹ W. Magnes,¹⁰ R.J. Strangeway,⁹ K.R. Bromund,¹¹ F. Plaschke,¹⁰ D. Fischer,¹⁰ H.K. Leinweber,⁹ B.J. Anderson,⁵ G. Le,¹¹ J.A. Slavin,¹³ E.L. Kepko,¹¹ W. Baumjohann,¹⁰ B. Mauk,³ S.A. Fuselier,¹³ and R. Nakamura,¹⁰

Corresponding author: H. Breuillard, Laboratoire de Physique des Plasmas, Université Pierre et Marie Curie, 4 place Jussieu, 75252 Paris, France. (hugo.breuillard@lpp.polytechnique.fr)

¹Laboratoire de Physique des Plasmas

This is the author manuscript accepted for publication and has undergone full peer review but has not been through the copyediting, typesetting, pagination and proofreading process, which may lead to differences between this version and the Version of Record. Please cite this article as doi: 10.1002/2016GL069188

D R A F T

June 1, 2016, 5:31pm

D R A F T

Key Points.

Magnetotail, Bursty Bulk Flows, Whistler
Waves

1 Dipolarization fronts (DFs), embedded in
2 bursty bulk flows (BBFs), play a crucial role
3 in Earth's plasmasheet dynamics because the
4 energy input from the solar wind is partly dis-
5 sipated in their vicinity. This dissipation is in
6 the form of strong low-frequency waves that
7 can heat and accelerate energetic electrons up
8 to the high latitude plasmasheet. However, the
9 dynamics of DF propagation and associated
10 low-frequency waves in the magnetotail are
11 still under debate due to instrumental limi-
12 tations and spacecraft separation distances.
13 In May 2015 the Magnetospheric Multiscale
14 (MMS) mission was in a string-of-pearls con-
15 figuration with an average inter-satellite dis-
16 tance of 160 km, which allows us to study in
17 detail the microphysics of DFs. Thus in this
18 letter we employ MMS data to investigate the

(LPP/CNRS UMR7648), Paris, France.

19 properties of dipolarization fronts propagat-
20 ing earthward and associated whistler-mode
21 wave emissions. We show that the spatial dy-
22 namics of DFs are below the ion gyroradius
23 scale in this region (~ 500 km), which can mod-
24 ify the dynamics of energetic ions ahead of the
25 DF (e.g. making their motion non-adiabatic).
26 We also show that whistler-wave dynamics have
27 a temporal scale of the order of the ion gyrope-
28 riod (a few seconds), indicating that the per-
29 pendicular temperature anisotropy can vary
30 on such time scales.

²Department of Physics and Astronomy,

1. Introduction

31 Transient fast flows of plasma are often observed for a large range of geocentric distances
32 in Earth's magnetotail, from -5 to about -30 Earth radii [*Ohtani et al.*, 2004]. They
33 are thought to be formed by reconnection of stretched field lines in the tail [*Runov et al.*,
34 2009; *Sitnov et al.*, 2009] and/or in interchange heads [*Pritchett and Coroniti*, 2011, 2013].
35 These bursty bulk flows (BBFs) are well correlated with substorm activity [see, e.g.,
36 *Juusola et al.*, 2011] and are an important mechanism of the flux transport in the tail
37 [*Baumjohann*, 1993; *Baumjohann et al.*, 2002; *Volwerk et al.*, 2008]. BBFs propagating
38 Earthward are associated with the dipolarization of the stretched magnetic field line [see
39 e.g., *Nakamura et al.*, 2002; *Runov et al.*, 2011, 2012], also called dipolarization front (DF),
40 that is embedded in these flows and separates the hot, tenuous high-speed flow from the
41 cold, dense and slowly convecting surrounding plasma. The typical scale of DFs in the
42 near-Earth magnetotail is of the order of the ion inertial length and Larmor radius [see
43 e.g. *Runov et al.*, 2011; *Fu et al.*, 2012a].

44 DFs are invariably associated with intense and broadband electromagnetic fluctuations,
45 from the ion cyclotron frequency to larger than the electron cyclotron frequency [see *Zhou*
46 *et al.*, 2009; *Khotyaintsev et al.*, 2011; *Huang et al.*, 2012; *Huang et al.*, 2015a; *Viberg*
47 *et al.*, 2014, and references therein]. Various wave modes have been identified, such as
48 lower-hybrid (LH) and whistler-mode waves. While LH waves are observed directly at the
49 DFs, whistler waves are generally detected in the flux pile-up region (FPR), i.e. behind the
50 DFs [*Khotyaintsev et al.*, 2011; *Deng et al.*, 2010; *Fu et al.*, 2014; *Li et al.*, 2015]. These

University of Delaware, Newark, USA.

51 waves, that are continually radiated outward from the BBFs to the auroral oval, are
52 found to be a very efficient plasma sheet energy loss process [*Chaston et al.*, 2012; *Ergun*
53 *et al.*, 2015], transferring the energy from the fields to the plasma [*Huang et al.*, 2015b;
54 *Angelopoulos et al.*, 2013]. Whistlers have been previously recorded onboard Cluster
55 [*Khotyaintsev et al.*, 2011; *Huang et al.*, 2012] and THEMIS [*Le Contel et al.*, 2009; *Deng*
56 *et al.*, 2010] and are thought to be generated by the perpendicular electron temperature
57 anisotropy resulting from betatron acceleration that occurs as the magnetic field strength
58 increases inside the FPR [see e.g. *Wu et al.*, 2013; *Fu et al.*, 2014; *Huang et al.*, 2015b; *Wu*
59 *et al.*, 2015]. *Deng et al.* [2010] investigated the properties (namely propagation angle,
60 degree of polarization and ellipticity) of whistler waves inside the magnetotail FPR, and
61 by analyzing Poynting flux, *Khotyaintsev et al.* [2011] have shown that these waves are
62 generated near the geomagnetic equator.

63 Recently, multi spacecraft missions such as Cluster and THEMIS have allowed study of
64 the detailed dynamics of BBFs. The fine structure of DFs has been investigated using the
65 tetrahedron configuration of Cluster constellation by *Fu et al.* [2012b] [see also *Schmid*
66 *et al.*, 2015]. They concluded that on a global scale DFs are tangential discontinuities,
67 although *Balikhin et al.* [2014] observed oscillations within a few DF magnetic ramps
68 which would indicate field-aligned currents causing the plasma to flow across DFs. The
69 radial separation along the magnetotail of the THEMIS fleet also helped to investigate the
70 spatial evolution of BBFs [*Runov et al.*, 2009; *Sergeev et al.*, 2009]. In particular, *Runov*

³Swedish Institute of Space Physics,

71 *et al.* [2009] showed [see also *Sitnov et al.*, 2009, 2013; *Fu et al.*, 2013; *Angelopoulos et al.*,
72 2013] that BBFs are consistent with magnetotail reconnection outflows and thus DFs
73 originate from pulses of reconnection. Front-like structures may also appear due to the
74 kinetic ballooning/interchange instability (BICI), forming finger-like structures [*Pritchett*
75 *and Coroniti*, 2010, 2013; *Pritchett et al.*, 2014]. However, reconnection and interchange
76 are not necessarily mutually exclusive, as the edge of a reconnection jet was shown to
77 be interchange unstable [e.g. *Nakamura et al.*, 2002; *Runov et al.*, 2012], and localized
78 reconnection could be triggered in the wake of interchange heads [*Pritchett and Coroniti*,
79 2011, 2013]. Nevertheless, the THEMIS inter-spacecraft separation distances are never
80 smaller than the typical ion inertial length (~ 500 km) in the tail and do not allow study
81 of the subprotonic dynamics of DFs.

82 In May 2015, the MMS [*Burch et al.*, 2016] constellation was in the near-Earth tail in a
83 string-of-pearl configuration, with a very small separation distance (~ 160 km) between
84 each spacecraft that allows us to study BBF propagation below ion scales. In this paper
85 we take advantage of this unique configuration to investigate the spatial evolution of
86 two DFs on 15 May 2015 and their associated whistler emissions. In Section 2 we first
87 determine the propagation properties of the two DFs and then we show the low-frequency
88 wave dynamics associated with this event. The results are discussed and summarized in
89 Section 3.

2. Data analysis

Uppsala, Sweden.

90 Fig.1 gives an overview of the events observed on May 15, 2015 from 03:07:00 to 03:13:00
91 UT by the four MMS spacecraft located at $[-11.7, 1.11, 1.14] R_E$ in GSE coordinates.
92 Because B_x is smaller than 10 nT, MMS was close to the magnetic equator. Only magnetic
93 and electric field waveforms (all three components of each are obtained from DFG [Russell
94 *et al.*, 2016], and ADP [Ergun *et al.*, 2016] and SDP [Lindqvist *et al.*, 2016] instruments,
95 respectively) as well as probe-to-spacecraft potential are presented in this figure, as FPI
96 [Fast Plasma Investigation, see Pollock *et al.*, 2016] instrument was turned off at this time
97 during the commissioning phase. Two dipolarization events can be distinguished at about
98 03:08:10 and 03:11:55 UT, characterized by a steep magnetic ramp of the B_z component
99 from -1 and 5 nT to 9 and 10 nT in about 8 and 5 s, respectively. The inclination of
100 the magnetic field increases simultaneously of about 40 and 25 degrees, respectively, and
101 the maximum inclination angle is $\theta_{max} \geq 45^\circ$ for both events. However, the first DF is
102 accompanied by a high-speed flow ($v \geq 150$ km/s) whereas the second DF is not. For
103 these two events, the behavior of the B_x component is similar (increase before and at the
104 B_z ramp), however it is opposite for B_y (B_y decreases at the second DF).

105 The variations of plasma density n , inferred from probe-to-spacecraft potential, are
106 also opposite for the two DFs: the density increases slightly at the first DF (at 03:07:50
107 UT) but then decreases (fluctuations of $|B|$ and n are out of phase, as in fast modes),
108 whereas at the second DF the density decreases at 03:11:50 UT and then increases behind
109 the DF (fluctuations of $|B|$ and n are in phase, as in slow modes). These two types of

⁴University of Colorado, Boulder, CO,

110 density signatures have been observed in statistical studies [*Schmid et al.*, 2011; *Schmid*
111 *et al.*, 2015] and the first DF seems to fall in categories A/D while the second DF falls
112 in category B/C in the classification established by *Schmid et al.* [2015]. In addition,
113 just before the first DF a very sharp potential (i.e., density) drop is observed, along with
114 a decrease/increase of B_z/B_x resulting in a slight increase of $|B|$ ahead of the magnetic
115 ramp (see Fig.1). These features are discussed in the following section.

116 We perform a minimum variance analysis [MVA, see e.g. *Sonnerup and Cahill*, 1967]
117 at the two DFs for all spacecraft to determine the propagation properties of the normal
118 to the front. The minimum variance directions (MVDs) calculated for the extent of the
119 magnetic ramp of the first DF are [0.55, -0.83, 0.07], [0.48, -0.87, 0.05], [0.46, -0.88, 0.04],
120 [0.43, -0.9, 0.03] for MMS1, MMS2, MMS3 and MMS4, respectively. The MVDs for the
121 first DF are well defined on all spacecraft with a ratio of the intermediate to minimum
122 eigenvalues in the range [8-10] and a ratio of maximum to intermediate eigenvalues in the
123 range [3-4]. The normal of the first DF is thus mostly directed along Y. For the second
124 DF the MVDs are less well defined, thus in this paper we choose to study in detail the
125 propagation properties of the first DF.

126 The normal to the first discontinuity (i.e. the direction of propagation of the first
127 DF) derived from the MVA performed on each spacecraft is sketched in Fig.2. The
128 normal of the first DF rotates significantly (the Y component decreases whereas the X
129 and Z components increase) between each spacecraft in the XY and XZ planes, i.e. on
130 a scale of ~ 500 km, during its earthward propagation. In the absence of bulk plasma

USA

131 measurements, we determine the velocity of the convected plasma of the FPR (where
 132 the plasma is convected and the Hall term is small [*Li et al.*, 2011; *Fu et al.*, 2012a]) in
 133 the MVA frame as $(E \times B)/B^2 \approx 150$ km/s and directed along the minimum variance
 134 direction for the first DF (see Fig.1e). Assuming the duration of the front (i.e. the
 135 magnetic ramp) as $\Delta t \approx 8$ s (see the B_z component in 1), we estimate the spatial scale
 136 (thickness) of the DF as $\Delta d \approx 1200$ km (i.e. $\sim 2.5\rho_i$, ρ_i being the ion gyroradius). The
 137 standard timing analysis [see Eq.12.9 from *Paschmann and Daly*, 1998] fails in our case
 138 (string-of-pearls configuration) because it requires the 4 spacecraft to be non-coplanar.
 139 However, the normals calculated for MMS4 and MMS3 are close to the plane determined
 140 by the alignment of the 4 spacecraft (see Fig.1), which is confirmed by the sequential
 141 observation of the DF by C4 and C3. The B_z profiles observed by MMS4 and MMS3
 142 are also very similar, meaning we can do the timing unambiguously. Thus, by simply
 143 time-shifting the B_z data from MMS4 and MMS3, we can estimate roughly the velocity
 144 of DF. We determine $\delta t \approx 1$ s between the 2 spacecraft and thus the velocity of the DF
 145 as $v_{DF} \equiv \delta d/\delta t \approx 160$ km/s along the spacecraft separation, with an uncertainty of ~ 50
 146 km/s. Taking into account the uncertainties on both velocity estimates ($E \times B/B^2$ and
 147 timing) the convective velocity and the discontinuity velocity can be considered as equal
 148 therefore the first DF can be characterized as a tangential discontinuity. These results
 149 and their probable causes are discussed in the following section.

⁵The Johns Hopkins University Applied

150 We also perform an analysis of E- and B-fields fluctuations in the frequency range [1-64]
151 Hz, i.e. between the ion and electron gyrofrequencies, obtained from ADP, SDP and SCM
152 [*Le Contel et al.*, 2016] instruments. The results of this analysis for MMS2 are summarized

Physics Laboratory, MD, USA.

⁶KTH Royal Institute of Technology,
Stockholm, Sweden.

⁷Southwest Research Institute, San
Antonio, TX, USA.

⁸University of New Hampshire, Durham,
NH, USA.

⁹Institute of Geophysics and Planetary
Physics/UCLA, Los Angeles, CA, USA.

¹⁰Space Research Institute
(IWF)/Austrian Academy of Sciences,
Graz, Austria.

¹¹NASA Goddard Space Flight Center,
Greenbelt, MD, USA.

¹²University of Michigan, Ann Arbor, MI,
USA.

¹³University of Texas at San Antonio, TX,
USA.

153 in Fig.3. We observe very strong electrostatic fluctuations close to the lower-hybrid (LH)
154 frequency exactly at the time of the first DF ($\sim 03:08:10$ UT). These are thus probably LH
155 waves, as inherently observed at DFs [*Deng et al.*, 2010; *Khotyaintsev et al.*, 2011; *Huang*
156 *et al.*, 2012]. Behind the first front we also observe strong electromagnetic fluctuations with
157 a frequency just above $0.1f_{ce}$ (white line in Fig.3, f_{ce} being the electron gyrofrequency)
158 and a highly (degree of polarization > 0.9) right-handed (ellipticity ≈ 1) polarized, as
159 well as a low propagation angle to the background magnetic field ($\theta \leq 20^\circ$). Thus, these
160 fluctuations are likely whistler waves, as often observed behind DFs [*Khotyaintsev et al.*,
161 2011; *Fu et al.*, 2014; *Viberg et al.*, 2014; *Li et al.*, 2015]. Weaker LH and whistler waves
162 are also observed at and behind the second DF ($\sim 03:11:55$ UT), which is also weaker in
163 ΔB_z . However, the whistlers behind the second DF propagate obliquely ($\theta \approx 40 - 50^\circ$) to
164 the background magnetic field. In addition, although most of whistlers propagate towards
165 the magnetic equator (anti-parallel Poynting flux), we observe whistlers with a reversed
166 Poynting flux (parallel to magnetic field) at about 03:08:45 UT, with less intensity as seen
167 on magnetic and electric spectra. These results are discussed in the following section as
168 well.

169 The same analysis was conducted on other spacecraft (not shown) resulting in similar
170 wave properties (degree of polarization, wave angle, ellipticity and Poynting flux) for
171 this time interval. However, there is a clear evolution of magnetic spectra observed at the
172 different spacecraft, as shown in Fig.4. The latter displays enhanced magnetic fluctuations
173 along the BBFs trajectory so that MMS1 (which is closer to the Earth, see Fig.2) observes
174 strong whistlers at 03:08:55 UT whereas MMS4 does not. Whistlers behind the second

DF are also stronger on MMS1 than on MMS4 (see Fig.4). This wave growth enhances the electromagnetic power by about 2 orders of magnitude (from about $2 \cdot 10^{-10}$ on MMS4 to $1 \cdot 10^{-8}$ W/m^2 on MMS1) behind the first DF and about 1 order of magnitude (from $\sim 1 \cdot 10^{-10}$ to $1 \cdot 10^{-9}$ W/m^2) behind the second DF, as seen on Fig.4. Fig.4 also shows that quasi-parallel whistlers at 03:08:55 UT are (about one order of magnitude) less intense than anti-parallel ones.

3. Summary and discussion

In May 2015, the newly launched MMS fleet was orbiting Earth in a string-of-pearls configuration. For the first time such configuration with very close spacecraft separation distance (~ 160 km) flew through the near-Earth magnetotail ($\sim 10 - 12R_E$). Making use of this unique opportunity, in this study we investigate the small-scale (i.e., below the ion gyroradius) dynamics of DFs propagation in the tail and their associated low-frequency emissions.

Our results can be summarized as follows: 1) two DF structures are identified, both generated at the magnetic equator and propagating earthward, but they are probably of different nature: based on the density variations therein, they fall into different categories of DFs [Schmid *et al.*, 2015]. 2) The first DF is probably a tangential discontinuity and is very dynamic: its normal rotates towards Earth on spatial scales less than the ion gyroradius (~ 500 km). 3) Both DFs show strong associated low-frequency waves (LH at DF and whistlers behind it) but with different properties: while intense quasi-parallel whistlers are observed behind the first DF, weaker oblique whistlers are observed behind the second one. 4) The dynamics of whistler waves associated with the first DF are also

196 subprotonic: in less than 5 seconds $|B|$ increases (i.e. the flux tube is compressed) as
197 the DF propagates earthward (from MMS4 to MMS1) and the whistler electromagnetic
198 power is enhanced by 1 to 2 orders of magnitude. Some wave packets are observed to
199 have a reversed (anti-parallel) Poynting flux within the FPR. However, these results raise
200 some questions that we discuss in the following paragraph.

201 As deduced from the MVA, the two DF events in this study seem to be generated in the
202 midtail (they propagate earthward) at the magnetic equator, in agreement with models
203 [*Runov et al.*, 2011; *Sitnov et al.*, 2013; *Nakamura et al.*, 2002; *Pritchett et al.*, 2014] and
204 previous observations [e.g. *Le Contel et al.*, 2009]. The normal of the first DF in the XZ
205 plane is first directed northward (XZ plane) and dawnward (XY plane) but then rotates
206 earthward (components in Y, Z directions decrease, X component increases) during its
207 propagation, on a spatial scale (~ 500 km) less than the ion gyroradius. This subprotonic-
208 scale rotation of the DF might for instance modify the dynamics of accelerated high-energy
209 particles in the vicinity of the DF (such as for instance reflected ions ahead of the DF as
210 described in [*Zhou et al.*, 2010]). Detailed analysis of such particle measurements using
211 MMS data and dedicated numerical simulations are thus necessary to determine the effects
212 on particle dynamics at these scales. The MVDs calculated for the first front are clearly
213 defined, in contrast with the MVDs calculated for the second DF; presumably because
214 the second DF is located in the "turbulent trail" of the first DF, as the magnetic field
215 from $\sim 03:09:50$ to $03:12:00$ UT appears to be highly fluctuating. Nevertheless, particle
216 measurements are needed to study turbulence in the vicinity of DF [*Huang et al.*, 2012]

217 and in BBFs [*Vrs et al.*, 2004; *Vörös et al.*, 2006], and this issue is thus beyond the scope
218 of this study.

219 The estimation of the bulk plasma (as deduced from $(E \times B)/B^2$) and discontinuity
220 (roughly estimated from timing analysis) velocities give rather similar values (~ 150
221 km/s) and the bulk velocity is directed along the front normal, thus this DF seems to be
222 a tangential discontinuity [*Schmid et al.*, 2011; *Fu et al.*, 2012b]. Additionally, fluctuations
223 in the magnetic ramp are weak, thus field-aligned currents at the DF must not be strong
224 and the plasma flow crossing the instability may not be significant [*Balikhin et al.*, 2014;
225 *Huang et al.*, 2015b]. In addition, a significant drop in density (inferred from probe-to-
226 spacecraft potential) over about 20s is observed about 30 s ahead of the first DF (at
227 $\sim 03:07:35$). This steep density hole is accompanied by a singular magnetic signature
228 (slight increase in B_x and decrease in B_z components, see Fig.1), whereas no particular
229 electric fluctuations are observed at this time (e.g. on MMS2, see Fig.3). This could be
230 the signature of the earthward propagation of a DF as a flux rope, as depicted in the
231 multiple reconnection X-lines (MRX) model [see e.g. *Lee*, 1995; *Slavin et al.*, 2003; *Huang*
232 *et al.*, 2015; *Lu et al.*, 2015]. In particular, *Lu et al.* [2015] have performed a 3D hybrid
233 simulation of DFs as earthward propagating flux ropes, and has shown that the multiple
234 X line reconnection process gives birth to flux ropes that propagate earthward with a B_z
235 and plasma density dip signature (as observed on Fig.1) ahead of them [see Fig.1b to e in
236 *Lu et al.*, 2015], especially if a previously formed flux rope is located closer to the Earth
237 [see Fig.1c in *Lu et al.*, 2015]. However, the exact nature of this phenomenon is still to
238 be determined and we leave this for future studies.

239 Intense low-frequency waves are also observed at (LH) and behind (whistlers) DFs. The
240 calculation of Poynting flux (see Fig.3) seems to indicate that they propagate towards the
241 magnetic equator. However, the presence of the two sudden reversals in their direction of
242 propagation and the fact that B_x oscillates around zero when they are observed, suggest
243 that the spacecraft are located in the whistler generation region close to the magnetic
244 equator [Le Contel et al., 2009; Runov et al., 2011]. This propagation direction is consis-
245 tent with the position of the spacecraft at that time ($Z_{GSE} \approx 1.14R_E$). Whistlers become
246 more intense closer to the Earth as $|B|$ increases from MMS4 to MMS1 when they are ob-
247 served, indicating that the perpendicular anisotropy may vary at the time scale of the ion
248 gyroperiod (~ 2 s). From 4 a very rough estimation of the growth rate gives $\gamma \approx 0.001\Omega_e$,
249 $\Omega_e \approx 200$ Hz being the electron gyro-pulsation (see right panels on Fig.4). This result is
250 consistent with growth rates calculated from models with similar plasma parameters [see
251 e.g. first plasma model from Le Contel et al., 2009]. However, to accurately determine
252 the temperature anisotropy, data particle are needed and we leave this for future study.

253 Whereas the whistlers at the first DF are quasi-parallel, those observed behind the
254 second front are oblique to the magnetic field. As stated above, the estimation of density
255 variations indicate that, according to Schmid et al. [2015] classification, the two DFs in this
256 study may be of different nature. Thus it might be possible that the properties of whistlers
257 associated with DFs are dependent on the nature of these DFs, as different pitch angle
258 distributions of suprathermal electrons have been observed behind different types of DFs
259 [Fu et al., 2011; Fu et al., 2012c]. However, a statistical study of low-frequency emissions
260 associated to DFs of different nature is necessary and is left for future investigation.

261 To conclude, the subprotonic dynamics of DFs (rotation of the normal on a scale ~ 500
262 km) and their associated low-frequency emissions (whistler waves intensification) in the
263 magnetotail are shown for the first time due to the small separation distance (~ 160 km) of
264 MMS string-of-pearls configuration in May 2015. Unfortunately, the FPI instruments were
265 not turned on at that time so only electromagnetic fields data are presented. Observations
266 in phase 1X (starting in March 2016) will also have FPI instruments turned on very
267 sparsely and moreover the apogee in the nightside will be located far from the magnetic
268 equator ($Z \approx 5R_E$). Thus the events shown in this paper represent a unique opportunity
269 to study the kinetic-scale dynamics of DF propagation and associated whistler emissions.

270 **Acknowledgments.** H.B.'s work has been supported by CNES through the grant
271 "Allocations de recherche post-doctorale". The French involvement (SCM) on MMS
272 is supported by CNES, CNRS-INSIS and CNRS-INSU. Used data are available at:
273 <https://lasp.colorado.edu/mms/sdc>

References

- 274 Angelopoulos, V., A. Runov, X.-Z. Zhou, D. L. Turner, S. A. Kiehas, S.-S. Li, and
275 I. Shinohara (2013), Electromagnetic energy conversion at reconnection fronts, *Science*,
276 *341*(6153), 1478–1482, doi:10.1126/science.1236992.
- 277 Balikhin, M. A., A. Runov, S. N. Walker, M. Gedalin, I. Dandouras, Y. Hobara, and
278 A. Fazakerley (2014), On the fine structure of dipolarization fronts, *Journal of Geo-*
279 *physical Research (Space Physics)*, *119*, 6367–6385, doi:10.1002/2014JA019908.

- 280 Baumjohann, W. (1993), The Near Earth Plasma Sheet - an AMPTE / IRM Perspective,
281 *Space Sci. Rev.*, *64*, 141–163, doi:10.1007/BF00819660.
- 282 Baumjohann, W., R. Schödel, and R. Nakamura (2002), Bursts of fast magneto-
283 tail flux transport, *Advances in Space Research*, *30*, 2241–2246, doi:10.1016/S0273-
284 1177(02)80234-4.
- 285 Burch, J. L., T. E. Moore, R. B. Torbert, and B. L. Giles (2016), Magnetospheric
286 multiscale overview and science objectives, *Space Science Reviews*, *199*(1), 5–21, doi:
287 10.1007/s11214-015-0164-9.
- 288 Chaston, C. C., J. W. Bonnell, L. Clausen, and V. Angelopoulos (2012), Energy transport
289 by kinetic-scale electromagnetic waves in fast plasma sheet flows, *Journal of Geophysical*
290 *Research (Space Physics)*, *117*, A09202, doi:10.1029/2012JA017863.
- 291 Deng, X., M. Ashour-Abdalla, M. Zhou, R. Walker, M. El-Alaoui, V. Angelopoulos, R. E.
292 Ergun, and D. Schriver (2010), Wave and particle characteristics of earthward electron
293 injections associated with dipolarization fronts, *Journal of Geophysical Research (Space*
294 *Physics)*, *115*, A09225, doi:10.1029/2009JA015107.
- 295 Ergun, R. E., K. A. Goodrich, J. E. Stawarz, L. Andersson, and V. Angelopoulos (2015),
296 Large-amplitude electric fields associated with bursty bulk flow braking in the earth's
297 plasma sheet, *Journal of Geophysical Research: Space Physics*, *120*(3), 1832–1844, doi:
298 10.1002/2014JA020165, 2014JA020165.
- 299 Ergun, R. E., S. Tucker, J. Westfall, K. A. Goodrich, D. M. Malaspina, D. Summers,
300 J. Wallace, M. Karlsson, J. Mack, N. Brennan, B. Pyke, P. Withnell, R. Torbert,
301 J. Macri, D. Rau, I. Dors, J. Needell, P.-A. Lindqvist, G. Olsson, and C. M. Cully

- 302 (2016), The axial double probe and fields signal processing for the mms mission, *Space*
303 *Science Reviews*, 199(1), 167–188, doi:10.1007/s11214-014-0115-x.
- 304 Fu, H. S., Y. V. Khotyaintsev, M. Andr, and A. Vaivads (2011), Fermi and betatron ac-
305 celeration of suprathermal electrons behind dipolarization fronts, *Geophysical Research*
306 *Letters*, 38(16), n/a–n/a, doi:10.1029/2011GL048528, 116104.
- 307 Fu, H. S., Y. V. Khotyaintsev, A. Vaivads, M. André, and S. Y. Huang (2012a), Occurrence
308 rate of earthward-propagating dipolarization fronts, *Geophys. Res. Lett.*, , 39, L10101,
309 doi:10.1029/2012GL051784.
- 310 Fu, H. S., Y. V. Khotyaintsev, A. Vaivads, M. André, and S. Y. Huang (2012b), Electric
311 structure of dipolarization front at sub-proton scale, *Geophys. Res. Lett.*, , 39, L06105,
312 doi:10.1029/2012GL051274.
- 313 Fu, H. S., Y. V. Khotyaintsev, A. Vaivads, M. André, V. A. Sergeev, S. Y. Huang, E. A.
314 Kronberg, and P. W. Daly (2012c), Pitch angle distribution of suprathermal electrons
315 behind dipolarization fronts: A statistical overview, *Journal of Geophysical Research*
316 (*Space Physics*), 117, A12221, doi:10.1029/2012JA018141.
- 317 Fu, H. S., J. B. Cao, Y. V. Khotyaintsev, M. I. Sitnov, A. Runov, S. Y. Fu, M. Hamrin,
318 M. André, A. Retinò, Y. D. Ma, H. Y. Lu, X. H. Wei, and S. Y. Huang (2013), Dipolar-
319 ization fronts as a consequence of transient reconnection: In situ evidence, *Geophys.*
320 *Res. Lett.*, , 40, 6023–6027, doi:10.1002/2013GL058620.
- 321 Fu, H. S., J. B. Cao, C. M. Cully, Y. V. Khotyaintsev, A. Vaivads, V. Angelopoulos,
322 Q.-G. Zong, O. Santolík, E. Macúšová, M. André, W. L. Liu, H. Y. Lu, M. Zhou, S. Y.
323 Huang, and Z. Zhima (2014), Whistler-mode waves inside flux pileup region: Structured

324 or unstructured?, *Journal of Geophysical Research (Space Physics)*, *119*, 9089–9100, doi:
325 10.1002/2014JA020204.

326 Huang, S. Y., M. Zhou, X. H. Deng, Z. G. Yuan, Y. Pang, Q. Wei, W. Su, H. M.
327 Li, and Q. Q. Wang (2012), Kinetic structure and wave properties associated with
328 sharp dipolarization front observed by cluster, *Annales Geophysicae*, *30*(1), 97–107,
329 doi:10.5194/angeo-30-97-2012.

330 Huang, S. Y., M. Zhou, F. Sahraoui, A. Vaivads, X. H. Deng, M. André, J. S. He, H. S.
331 Fu, H. M. Li, Z. G. Yuan, and D. D. Wang (2012), Observations of turbulence within
332 reconnection jet in the presence of guide field, *Geophys. Res. Lett.*, *39*, L11,104, doi:
333 10.1029/2012GL052210.

334 Huang, S. Y., Z. G. Yuan, B. Ni, M. Zhou, H. S. Fu, S. Fu, X. H. Deng, Y. Pang, H. M.
335 Li, D. D. Wang, H. M. Li, and X. D. Yu (2015a), Observations of large-amplitude
336 electromagnetic waves and associated wave-particle interactions at the dipolarization
337 front in the Earth's magnetotail: A case study, *Journal of Atmospheric and Solar-*
338 *Terrestrial Physics*, *129*, 119–127, doi:10.1016/j.jastp.2015.05.007.

339 Huang, S. Y., H. S. Fu, Z. G. Yuan, M. Zhou, S. Fu, X. H. Deng, W. J. Sun, Y. Pang, D. D.
340 Wang, H. M. Li, H. M. Li, and X. D. Yu (2015b), Electromagnetic energy conversion at
341 dipolarization fronts: Multispacecraft results, *Journal of Geophysical Research (Space*
342 *Physics)*, *120*, 4496–4502, doi:10.1002/2015JA021083.

343 Huang, S. Y., M. Zhou, Z. G. Yuan, H. S. Fu, J. S. He, F. Sahraoui, N. Aunai, X. H. Deng,
344 S. Fu, Y. Pang, and D. D. Wang (2015), Kinetic simulations of secondary reconnection
345 in the reconnection jet, *Journal of Geophysical Research: Space Physics*, *120*(8), 6188–

- 346 6198, doi:10.1002/2014JA020969, 2014JA020969.
- 347 Juusola, L., N. ØStgaard, E. Tanskanen, N. Partamies, and K. Snekvik (2011), Earthward
348 plasma sheet flows during substorm phases, *Journal of Geophysical Research (Space
349 Physics)*, *116*, A10228, doi:10.1029/2011JA016852.
- 350 Khotyaintsev, Y. V., C. M. Cully, A. Vaivads, M. André, and C. J. Owen (2011), Plasma
351 jet braking: Energy dissipation and nonadiabatic electrons, *Phys. Rev. Lett.*, *106*,
352 165,001, doi:10.1103/PhysRevLett.106.165001.
- 353 Le Contel, O., A. Roux, C. Jacquy, P. Robert, M. Berthomier, T. Chust, B. Grison,
354 V. Angelopoulos, D. Sibeck, C. C. Chaston, C. M. Cully, B. Ergun, K.-H. Glassmeier,
355 U. Auster, J. McFadden, C. Carlson, D. Larson, J. W. Bonnell, S. Mende, C. T. Russell,
356 E. Donovan, I. Mann, and H. Singer (2009), Quasi-parallel whistler mode waves observed
357 by themis during near-earth dipolarizations, *Annales Geophysicae*, *27*(6), 2259–2275,
358 doi:10.5194/angeo-27-2259-2009.
- 359 Le Contel, O., P. Leroy, A. Roux, C. Coillot, D. Alison, A. Bouabdellah, L. Mirioni,
360 L. Meslier, A. Galic, M. C. Vassal, R. B. Torbert, J. Needell, D. Rau, I. Dors, R. E.
361 Ergun, J. Westfall, D. Summers, J. Wallace, W. Magnes, A. Valavanoglou, G. Olsson,
362 M. Chutter, J. Macri, S. Myers, S. Turco, J. Nolin, D. Bodet, K. Rowe, M. Tanguy,
363 and B. de la Porte (2016), The Search-Coil Magnetometer for MMS, *Space Sci. Rev.*,
364 *199*, 257–282, doi:10.1007/s11214-014-0096-9.
- 365 Lee, L. C. (1995), A Review of Magnetic Reconnection: MHD Models, *Washington DC
366 American Geophysical Union Geophysical Monograph Series*, *90*, 139.

- 367 Li, H., M. Zhou, X. Deng, Z. Yuan, L. Guo, X. Yu, Y. Pang, and S. Huang (2015), A sta-
368 tistical study on the whistler waves behind dipolarization fronts, *Journal of Geophysical*
369 *Research (Space Physics)*, *120*, 1086–1095, doi:10.1002/2014JA020474.
- 370 Li, W., J. Bortnik, R. M. Thorne, and V. Angelopoulos (2011), Global distribution of wave
371 amplitudes and wave normal angles of chorus waves using THEMIS wave observations,
372 *J. Geophys. Res.*, , *116*, A12205, doi:10.1029/2011JA017035.
- 373 Lindqvist, P.-A., G. Olsson, R. B. Torbert, B. King, M. Granoff, D. Rau, G. Needell,
374 S. Turco, I. Dors, P. Beckman, J. Macri, C. Frost, J. Salwen, A. Eriksson, L. Åhlén,
375 Y. V. Khotyaintsev, J. Porter, K. Lappalainen, R. E. Ergun, W. Wernmeier, and S. Tucker
376 (2016), The spin-plane double probe electric field instrument for mms, *Space Science*
377 *Reviews*, *199*(1), 137–165, doi:10.1007/s11214-014-0116-9.
- 378 Lu, S., Q. Lu, Y. Lin, X. Wang, Y. Ge, R. Wang, M. Zhou, H. Fu, C. Huang, M. Wu, and
379 S. Wang (2015), Dipolarization fronts as earthward propagating flux ropes: A three-
380 dimensional global hybrid simulation, *Journal of Geophysical Research: Space Physics*,
381 *120*(8), 6286–6300, doi:10.1002/2015JA021213, 2015JA021213.
- 382 Nakamura, M. S., H. Matsumoto, and M. Fujimoto (2002), Interchange instabil-
383 ity at the leading part of reconnection jets, *Geophys. Res. Lett.*, , *29*, 1247, doi:
384 10.1029/2001GL013780.
- 385 Ohtani, S.-I., M. A. Shay, and T. Mukai (2004), Temporal structure of the fast con-
386 vective flow in the plasma sheet: Comparison between observations and two-fluid
387 simulations, *Journal of Geophysical Research (Space Physics)*, *109*, A03210, doi:
388 10.1029/2003JA010002.

389 Paschmann, G., and P. W. Daly (1998), Analysis Methods for Multi-Spacecraft Data.
390 ISSI Scientific Reports Series SR-001, ESA/ISSI, Vol. 1. ISBN 1608-280X, 1998, *ISSI*
391 *Scientific Reports Series, 1*.

392 Pollock, C., T. Moore, A. Jacques, J. Burch, U. Gliese, Y. Saito, T. Omoto, L. Avanov,
393 A. Barrie, V. Coffey, J. Dorelli, D. Gershman, B. Giles, T. Rosnack, C. Salo, S. Yokota,
394 M. Adrian, C. Aoustin, C. Auletta, S. Aung, V. Bigio, N. Cao, M. Chandler, D. Chornay,
395 K. Christian, G. Clark, G. Collinson, T. Corris, A. DeLosSantos, R. Devlin, T. Diaz,
396 T. Dickerson, C. Dickson, A. Diekmann, F. Diggs, C. Duncan, A. Figueroa-Vinas,
397 C. Firman, M. Freeman, N. Galassi, K. Garcia, G. Goodhart, D. Guererro, J. Hageman,
398 J. Hanley, E. Hemminger, M. Holland, M. Hutchins, T. James, W. Jones, S. Kreisler,
399 J. Kujawski, V. Lavu, J. Lobell, E. LeCompte, A. Lukemire, E. MacDonald, A. Mariano,
400 T. Mukai, K. Narayanan, Q. Nguyen, M. Onizuka, W. Paterson, S. Persyn, B. Piep-
401 grass, F. Cheney, A. Rager, T. Raghuram, A. Ramil, L. Reichenthal, H. Rodriguez,
402 J. Rouzaud, A. Rucker, M. Samara, J.-A. Sauvaud, D. Schuster, M. Shappirio, K. Shel-
403 ton, D. Sher, D. Smith, K. Smith, S. Smith, D. Steinfeld, R. Szymkiewicz, K. Tanimoto,
404 J. Taylor, C. Tucker, K. Tull, A. Uhl, J. Vloet, P. Walpole, S. Weidner, D. White,
405 G. Winkert, P.-S. Yeh, and M. Zeuch (2016), Fast plasma investigation for magneto-
406 spheric multiscale, *Space Science Reviews*, pp. 1–76, doi:10.1007/s11214-016-0245-4.

407 Pritchett, P. L., and F. V. Coroniti (2010), A kinetic ballooning/interchange instability
408 in the magnetotail, *Journal of Geophysical Research (Space Physics)*, 115, A06301, doi:
409 10.1029/2009JA014752.

- 410 Pritchett, P. L., and F. V. Coroniti (2011), Plasma sheet disruption by interchange-
411 generated flow intrusions, *Geophys. Res. Lett.*, , *38*, L10102, doi:10.1029/2011GL047527.
- 412 Pritchett, P. L., and F. V. Coroniti (2013), Structure and consequences of the kinetic
413 ballooning/interchange instability in the magnetotail, *Journal of Geophysical Research*
414 (*Space Physics*), *118*, 146–159, doi:10.1029/2012JA018143.
- 415 Pritchett, P. L., F. V. Coroniti, and Y. Nishimura (2014), The kinetic bal-
416 looning/interchange instability as a source of dipolarization fronts and auroral
417 streamers, *Journal of Geophysical Research (Space Physics)*, *119*, 4723–4739, doi:
418 10.1002/2014JA019890.
- 419 Runov, A., V. Angelopoulos, M. I. Sitnov, V. A. Sergeev, J. Bonnell, J. P. McFad-
420 den, D. Larson, K.-H. Glassmeier, and U. Auster (2009), THEMIS observations of
421 an earthward-propagating dipolarization front, *Geophys. Res. Lett.*, , *36*, L14106, doi:
422 10.1029/2009GL038980.
- 423 Runov, A., V. Angelopoulos, M. Sitnov, V. A. Sergeev, R. Nakamura, Y. Nishimura, H. U.
424 Frey, J. P. McFadden, D. Larson, J. Bonnell, K.-H. Glassmeier, U. Auster, M. Connors,
425 C. T. Russell, and H. J. Singer (2011), Dipolarization fronts in the magnetotail plasma
426 sheet, *Planet. Space Sci.*, *59*, 517–525, doi:10.1016/j.pss.2010.06.006.
- 427 Runov, A., V. Angelopoulos, and X.-Z. Zhou (2012), Multipoint observations of dipolar-
428 ization front formation by magnetotail reconnection, *Journal of Geophysical Research*
429 (*Space Physics*), *117*, A05230, doi:10.1029/2011JA017361.
- 430 Runov, A., V. Angelopoulos, C. Gabrielse, X.-Z. Zhou, D. Turner, and F. Plaschke (2013),
431 Electron fluxes and pitch-angle distributions at dipolarization fronts: Themis multipoint

432 observations, *Journal of Geophysical Research: Space Physics*, *118*(2), 744–755, doi:
433 10.1002/jgra.50121.

434 Russell, C. T., B. J. Anderson, W. Baumjohann, K. R. Bromund, D. Dearborn, D. Fis-
435 cher, G. Le, H. K. Leinweber, D. Leneman, W. Magnes, J. D. Means, M. B. Moldwin,
436 R. Nakamura, D. Pierce, F. Plaschke, K. M. Rowe, J. A. Slavin, R. J. Strangeway,
437 R. Torbert, C. Hagen, I. Jernej, A. Valavanoglou, and I. Richter (2016), The mag-
438 netospheric multiscale magnetometers, *Space Science Reviews*, *199*(1), 189–256, doi:
439 10.1007/s11214-014-0057-3.

440 Schmid, D., M. Volwerk, R. Nakamura, W. Baumjohann, and M. Heyn (2011), A statis-
441 tical and event study of magnetotail dipolarization fronts, *Annales Geophysicae*, *29*(9),
442 1537–1547, doi:10.5194/angeo-29-1537-2011.

443 Schmid, D., R. Nakamura, F. Plaschke, M. Volwerk, and W. Baumjohann (2015), Two
444 states of magnetotail dipolarization fronts: A statistical study, *Journal of Geophysical*
445 *Research (Space Physics)*, *120*, 1096–1108, doi:10.1002/2014JA020380.

446 Sergeev, V., V. Angelopoulos, S. Apatenkov, J. Bonnell, R. Ergun, R. Nakamura,
447 J. McFadden, D. Larson, and A. Runov (2009), Kinetic structure of the sharp injec-
448 tion/dipolarization front in the flow-braking region, *Geophys. Res. Lett.*, , *36*, L21105,
449 doi:10.1029/2009GL040658.

450 Sitnov, M. I., M. Swisdak, and A. V. Divin (2009), Dipolarization fronts as a signature
451 of transient reconnection in the magnetotail, *Journal of Geophysical Research (Space*
452 *Physics)*, *114*, A04202, doi:10.1029/2008JA013980.

- 453 Sitnov, M. I., N. Buzulukova, M. Swisdak, V. G. Merkin, and T. E. Moore (2013), Spon-
454 taneous formation of dipolarization fronts and reconnection onset in the magnetotail,
455 *Geophys. Res. Lett.*, , 40, 22–27, doi:10.1029/2012GL054701.
- 456 Slavin, J. A., R. P. Lepping, J. Gjerloev, D. H. Fairfield, M. Hesse, C. J. Owen, M. B.
457 Moldwin, T. Nagai, A. Ieda, and T. Mukai (2003), Geotail observations of magnetic
458 flux ropes in the plasma sheet, *Journal of Geophysical Research (Space Physics)*, 108,
459 1015, doi:10.1029/2002JA009557.
- 460 Sonnerup, B. U. ., and L. J. Cahill (1967), Magnetopause structure and attitude
461 from explorer 12 observations, *Journal of Geophysical Research*, 72(1), 171–183, doi:
462 10.1029/JZ072i001p00171.
- 463 Viberg, H., Y. V. Khotyaintsev, A. Vaivads, M. André, H. S. Fu, and N. Cornilleau-
464 Wehrlin (2014), Whistler mode waves at magnetotail dipolarization fronts, *Journal of*
465 *Geophysical Research (Space Physics)*, 119, 2605–2611, doi:10.1002/2014JA019892.
- 466 Volwerk, M., A. T. Y. Lui, M. Lester, A. P. Walsh, I. Alexeev, X. Cao, M. W. Dunlop,
467 A. N. Fazakerley, A. Grocott, L. Kistler, X. Lun, C. Mouikis, Z. Pu, C. Shen, J. K. Shi,
468 M. G. G. T. Taylor, W. Baumjohann, R. Nakamura, A. Runov, Z. Vörös, T. L. Zhang,
469 T. Takada, H. Rème, B. Klecker, and C. M. Carr (2008), Magnetotail dipolarization and
470 associated current systems observed by Cluster and Double Star, *Journal of Geophysical*
471 *Research (Space Physics)*, 113, A08S90, doi:10.1029/2007JA012729.
- 472 Vörös, Z., W. Baumjohann, R. Nakamura, M. Volwerk, and A. Runov (2006), Bursty Bulk
473 Flow Driven Turbulence in the Earth’s Plasma Sheet, *Space Sci. Rev.*, 122, 301–311,
474 doi:10.1007/s11214-006-6987-7.

- 475 Vrs, Z., W. Baumjohann, R. Nakamura, M. Volwerk, A. Runov, T. L. Zhang, H. U. Eichel-
476 berger, R. Treumann, E. Georgescu, A. Balogh, B. Klecker, and H. Rme (2004), Mag-
477 netic turbulence in the plasma sheet, *Journal of Geophysical Research: Space Physics*,
478 *109*(A11), n/a–n/a, doi:10.1029/2004JA010404, a11215.
- 479 Wu, M., M. Volwerk, Q. Lu, Z. Vrs, R. Nakamura, and T. Zhang (2013), The proton
480 temperature anisotropy associated with bursty bulk flows in the magnetotail, *Journal*
481 *of Geophysical Research: Space Physics*, *118*(8), 4875–4883, doi:10.1002/jgra.50451.
- 482 Wu, M., C. Huang, Q. Lu, M. Volwerk, R. Nakamura, Z. Vrs, T. Zhang, and S. Wang
483 (2015), In situ observations of multistage electron acceleration driven by magnetic re-
484 connection, *Journal of Geophysical Research: Space Physics*, *120*(8), 6320–6331, doi:
485 10.1002/2015JA021165, 2015JA021165.
- 486 Zhou, M., M. Ashour-Abdalla, X. Deng, D. Schriver, M. El-Alaoui, and Y. Pang
487 (2009), THEMIS observation of multiple dipolarization fronts and associated wave
488 characteristics in the near-Earth magnetotail, *Geophys. Res. Lett.*, , *36*, L20107, doi:
489 10.1029/2009GL040663.
- 490 Zhou, X.-Z., V. Angelopoulos, V. A. Sergeev, and A. Runov (2010), Accelerated ions
491 ahead of earthward propagating dipolarization fronts, *Journal of Geophysical Research:*
492 *Space Physics*, *115*(A5), n/a–n/a, doi:10.1029/2010JA015481, a00I03.



Figure 1. Summary of DFG and EDP measurements onboard the four MMS spacecraft, on the 15th of May 2015 between 03:06:00 and 03:14:00 UT. From top to bottom panels are: the modulus of magnetic field B , the x , y and z components, the convected plasma velocity ($\vec{E} \times \vec{B}$) along the DF normal and the probe-to-spacecraft potential.



Figure 2. Sketch (not on scale) of the MVDs of the first DF obtained onboard all four MMS spacecraft, in the equatorial XY (left panel) and meridional XZ (right panel) planes in GSM coordinates. The gray arrows depict the DF propagation inferred from the MVDs for the sake of clarity.




Fig3-eps-converted-to.pdf

Figure 3. Example of detailed wave analysis performed on MMS2 in the frequency range [1-64] Hz: the magnetic (panel a) and electric (panel b) field waveforms from DFG and EDP instruments in DMPA and DSL coordinates, respectively, are color coded. The time-frequency spectrograms computed from these waveforms are shown in panels c and d, respectively. The degree of polarization, propagation angle θ_k (between \vec{k} and \vec{B}_0), ellipticity and Poynting flux angle θ_S (between \vec{S} and \vec{B}_0) are also displayed in panels e, f, g and h, respectively.

D R A F T

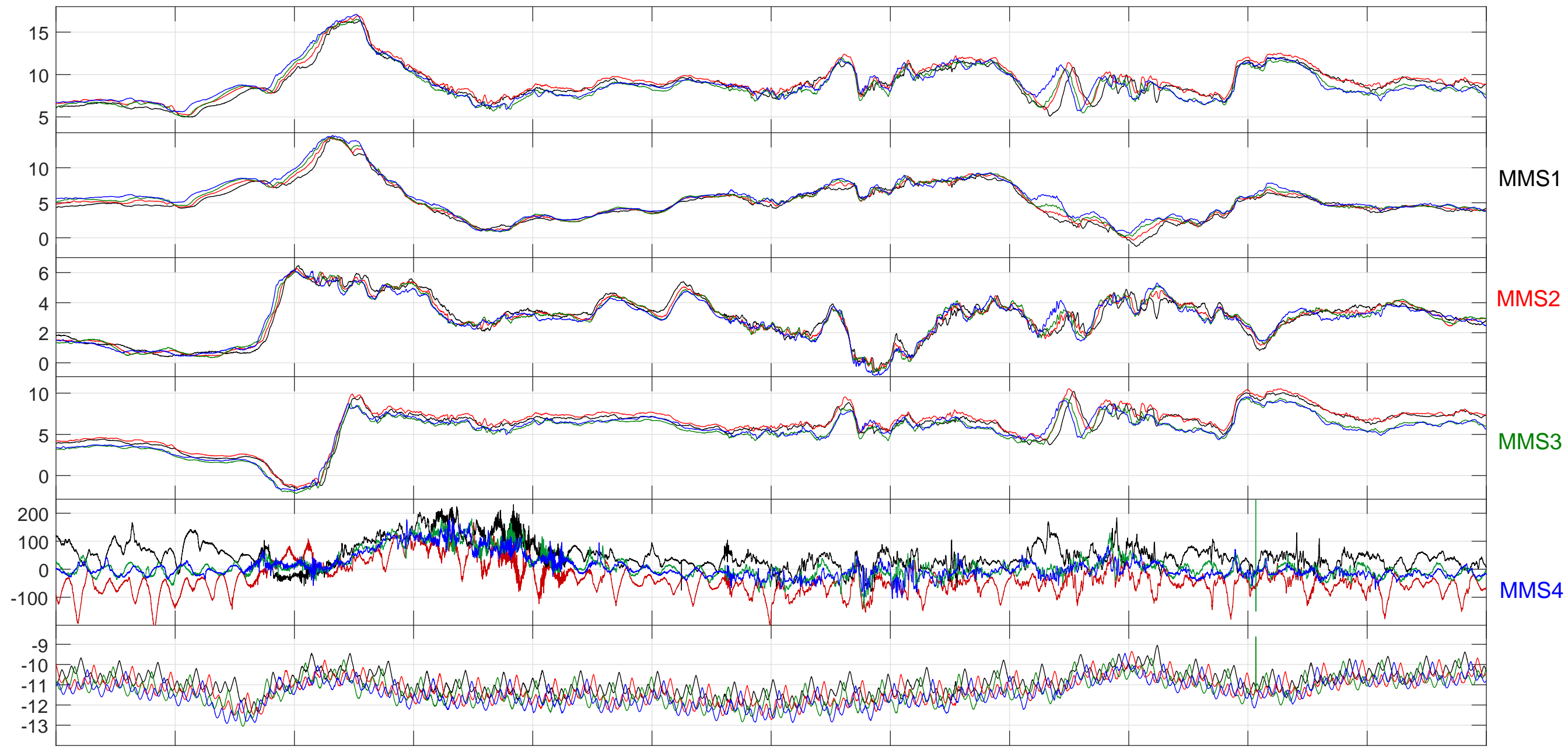
June 1, 2016, 5:31pm

D R A F T

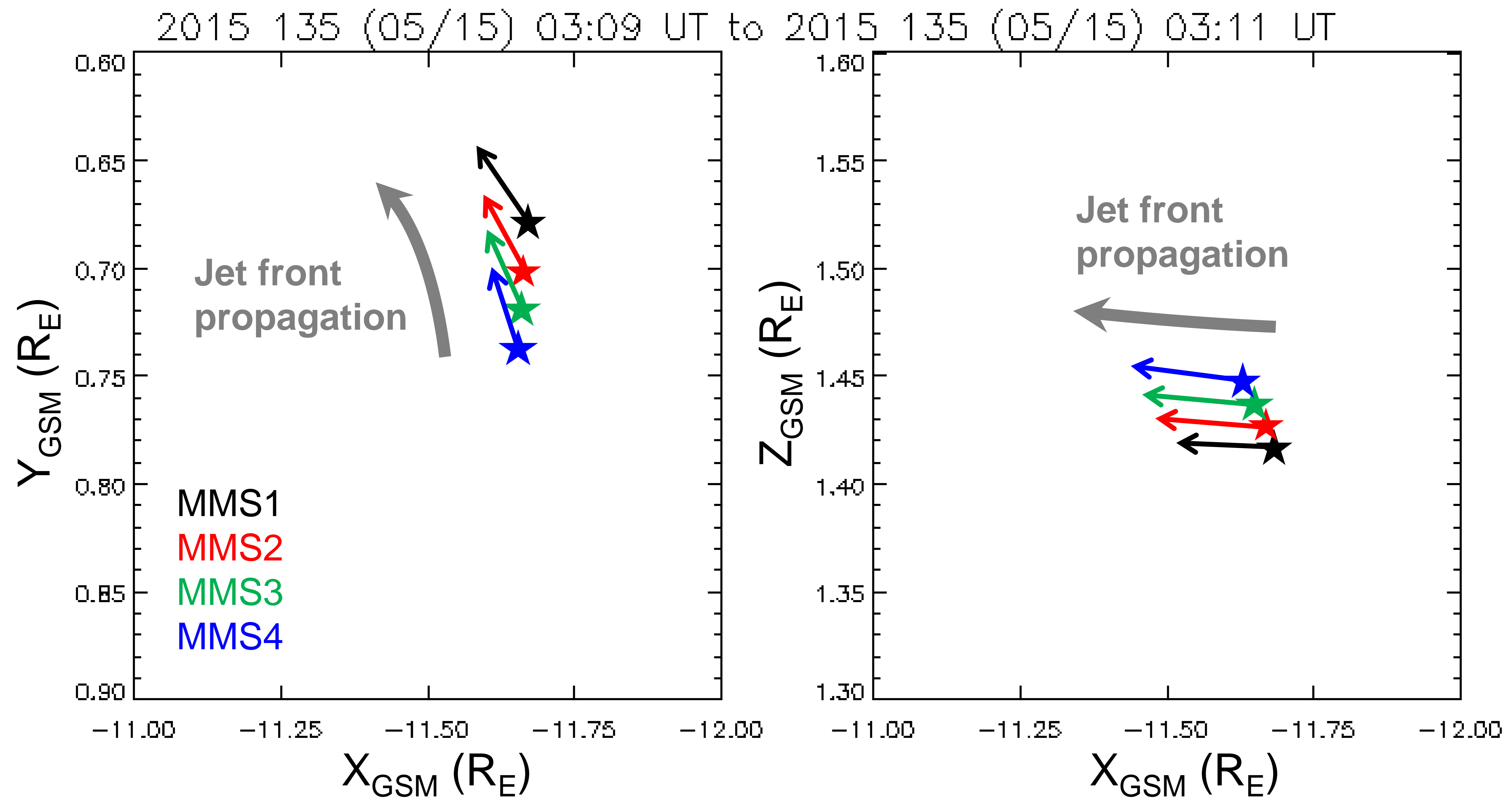


Figure 4. The total electromagnetic power (irradiance), computed from the Poynting flux, is shown (left panels) for all four spacecraft (from top to bottom MMS 1, 2, 3, 4) along the DF propagation (gray arrow). A zoom-in on 03:08:15 to 03:09:30 UT for each spacecraft (right panels) shows the evolution of time-frequency spectrograms of whistler waves.

2015-05-15

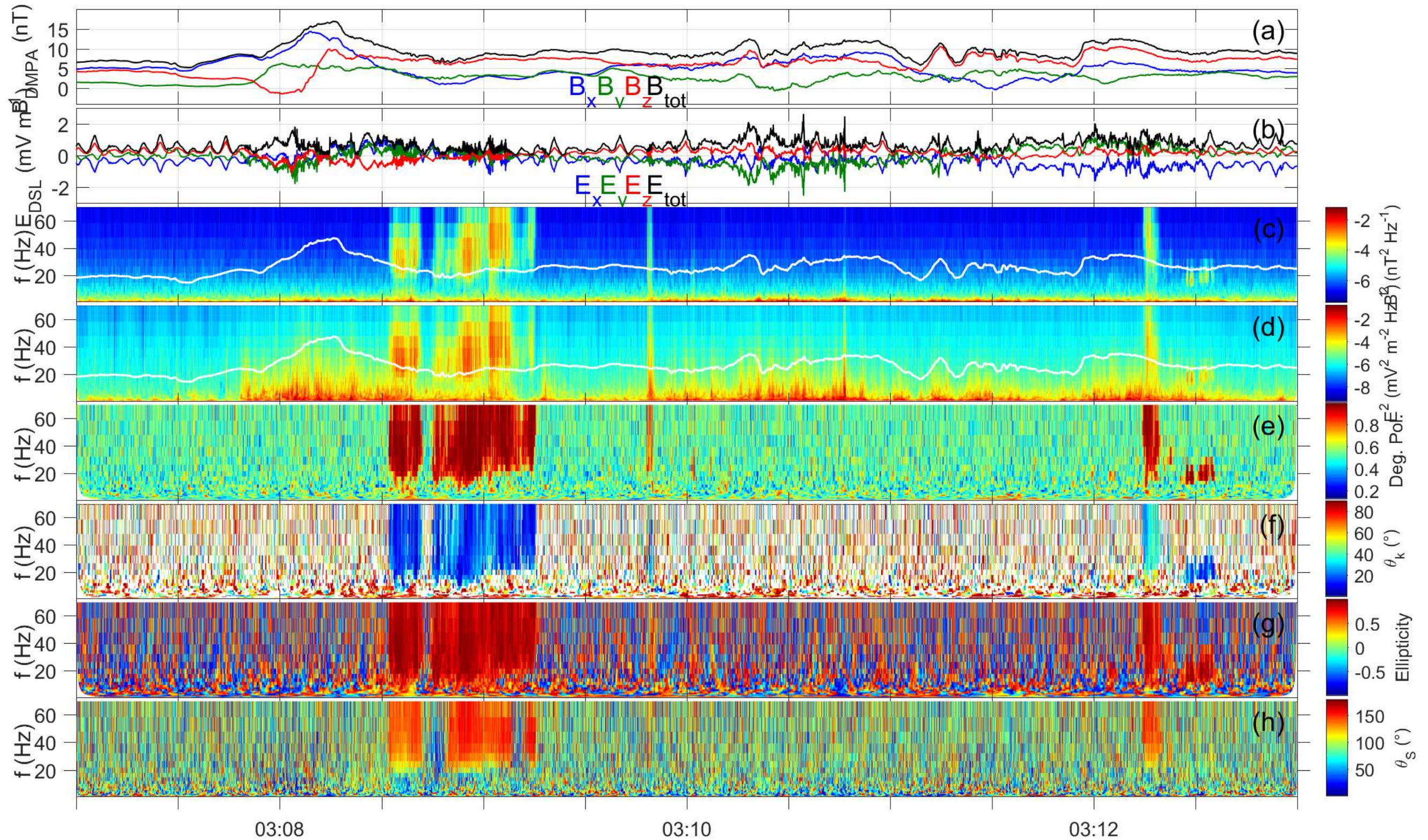


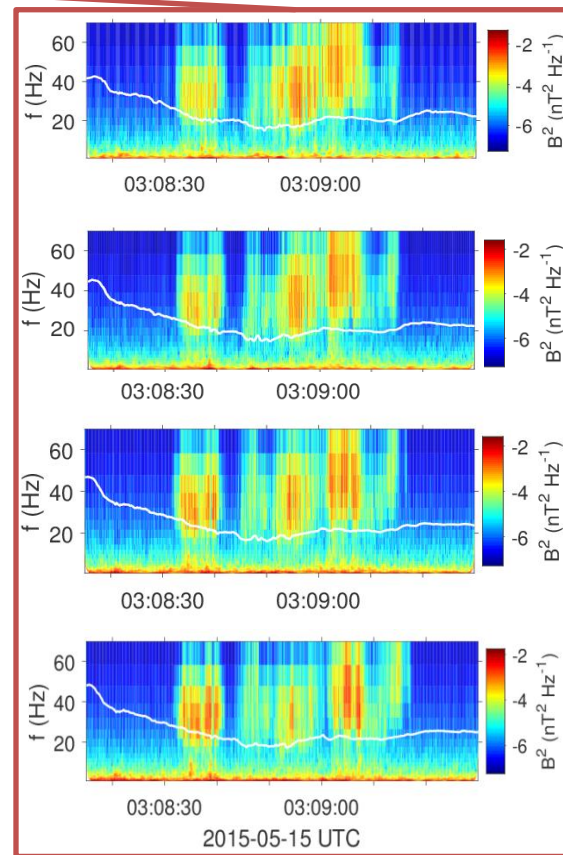
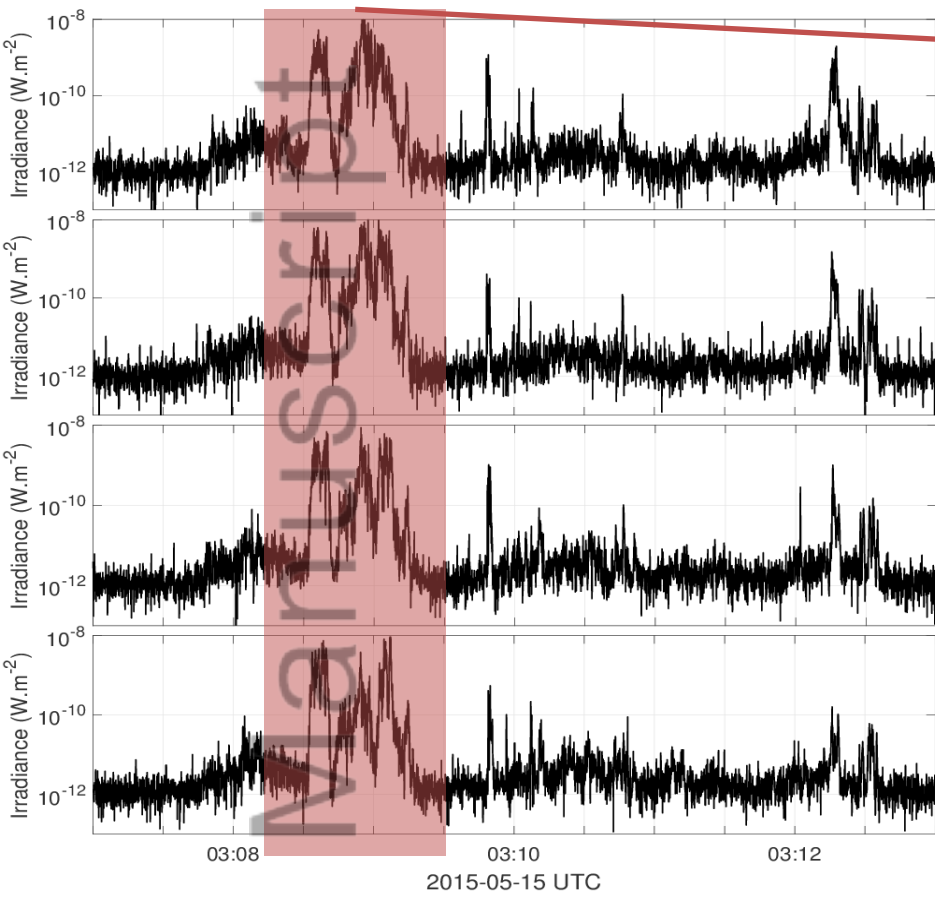
UT	03:08	03:10	03:12
X [Re]	-11.7	-11.7	-11.7
Y [Re]	1.12	1.11	1.09
Z [Re]	1.14	1.14	1.13
R [Re]	11.8	11.8	11.8



MMS2 - E&B analysis

Author Manuscript





MMS1

MMS2

MMS3

MMS4



DF propagation

Author